Modelling non-isothermal volume change and solute transport behaviours of a semi-permeable clay soil under the combined influence of mechanical loading, chemical-osmosis, and thermo-osmosis

Zhihong Zhang[1], Shakil A. Masum[2], Gailei Tian[1], Hywel R. Thomas[2]*

1 Key Laboratory of Urban Security & Disaster Engineering, Ministry of Education, Beijing University of Technology, Beijing 100124, People's Republic of China

2 Geoenvironmental Research Centre, Cardiff University, Cardiff CF24 3AA, UK

**Corresponding author: tiangailei@emails.bjut.edu.cn*

Abstract: Clays are widely used in geotechnical and geoenvironmental engineering applications and it is crucial to understand its behaviour for the dynamic field conditions. The presence of a temperature gradient across clayey soils that exhibit semi-permeable membrane (or osmotic) behaviour may promote a number of complex processes, including thermal expansion or consolidation, thermally induced osmosis, thermal diffusion, along with other flow and deformation processes. Chemical-osmosis and chemico-osmotic consolidation that are significant in isothermal conditions are also affected by temperature. Publications on chemical-osmosis, and to some extent thermo-osmosis behaviour of semi-permeable clays under coupled conditions are widely available. However, studies that include the influence of both thermo-osmosis and chemical-osmosis together are rare. In this paper, a fully coupled numerical model is presented to study the effects of both osmotic processes on thermo-hydro-mechanical-chemical behaviour of semi-permeable clays. Solute spread in a landfill clay liner is investigated under the

combined influence of mechanical, thermal, and chemical loading. Model results show that the clay deformation is sensitive to thermo-osmosis; and the effects of thermo-osmotic consolidation, excess pore water dissipation, and the overall settlement increases with temperature. Variation of the source temperature from 40℃ to 80℃ yielded an increase of 11.3% of the peak soil settlement. Significant contribution of thermo-osmosis on solute transport is noticed in this study and ignoring the process substantially deviate from the realism. Up to 80% overprediction of cadmium spread is observed in the clay liner when the thermo-osmotic processes are neglected.

Keywords: coupled transport, deformation, temperature, osmotic conductivity, thermo-osmotic conductivity, sorption.

1 Introduction

Clayey soils are often used as buffer materials to prevent and to minimise the spread of toxic pollutants in the surrounding environment. Materials such as synthetic or natural clay liners, compacted clays, often constitute the key component of engineered barrier systems (Coo et al., 2016) in various waste disposal and landfill applications. Efficacy of such systems depends largely on ensuring the expected physical, chemical and mechanical behaviour of clay buffers in-field or in-situ conditions (Zheng et al, 2017), where they are exposed to simultaneous thermal, hydraulic, chemical and mechanical loading events. Therefore, it is essential to study their complex, coupled flow and deformation behaviours on mitigating contaminant spread effectively and/ maintaining contamination level below regulatory limits.

Coupled flow and deformation processes in clays that exhibit semi-permeable membrane behaviour

are complex and strongly affected by the osmotic processes related to the physico-chemical interactions between the clay aggregates and the pore fluid (Barbour and Fredlund, 1989). During osmosis fluid flows through a semi-permeable membrane submitted to pore fluid chemicals (solutes) concentration gradients (Mitchell, 1973; Keijzer, 1997; Malusis, 2003) or to soil thermal gradient (Mitchell and Soga, 2005); and may lead to volumetric changes in the soil. The former is known as chemical-osmosis and the later as thermo-osmosis. The corresponding soil deformations are termed as chemico-osmotic consolidation (Mitchell, 1973; Kaczmarek and Hueckel, 1998) and thermo-osmotic consolidation (Mitchell and Soga, 2005). Osmotic potentials in clays depend on the osmotic efficiency of the membrane (ω), which varies between $0 \leq \omega \leq 1$ (Shackelford et al., 2019). Unlike perfect semi-permeable membranes, *i.e.* $\omega = 1$, clays exhibit imperfect semi-permeable behaviour and that leads to solute as well as pore fluids flow across the membrane (Barbour and Fredlund, 1989). When exposed to heating both soil aggregates and pore fluid experience thermal dilation; and under drained condition, the thermally induced expansion and expulsion of pore fluid across the membrane result into consolidation of the soil volume (Paaswell, 1967; Habibagahi, 1977; Delage, 2000; Monfared et al., 2012; Donna and Laloui, 2015). Pore fluid flow in semi-permeable clays during chemical-osmosis and thermo-osmosis are measured by the osmotic conductivity (k_ω) and the thermo-osmotic conductivity (k_T), respectively (Goncalves et al., 2012; Shackelford et al., 2019). When submitted to simultaneous thermal, hydraulic and chemical gradients, they combinedly contribute with the hydraulic conductivity (k_h) into the bulk fluid flow. Accurate prediction/ estimation of transport and fate of solutes in semi-permeable clays, therefore, depends on comprehensive understanding of the combined, inter-related flow and deformation behaviours.

Numerous studies on coupled processes in clayey soils are available in the literature. Here the focus is on the theoretical and/ numerical studies including coupled thermal, hydraulic, mechanical and/

chemical processes in semi-permeable clays with particular relevance to osmotically induced volume change behaviours. For isothermal conditions, the effects of chemical-osmosis and chemico-osmotic consolidations on coupled flow processes are presented in the works of Mitchell et al. (1973), Barbour and Fredlund (1989), Kaczmarek and Hueckel (1998), Malusis and Shackelford (2002), Peters and Smith (2004), Lewis et al. (2009), Pu et al. (2016), Xie et al. (2015), Zhang et al. (2018) and others (a comprehensive list of the literatures are available in Zhang et al. (2018)). However, the contribution of thermo-osmosis on coupled flow processes is usually ignored based on the assumption that the thermo-osmotic flux is negligible (Sánchez, et al., 2016; Shackelford et al., 2019). For argillaceous media *e.g.* semi-impermeable clays, validity of this assumption is questionable (Soler, 2001; Shackelford et al., 2019). Laboratory investigations on non-isothermal volume change experiments in clays, (Carnahan, 1983; McVay, 1984, Delage et al., 2000; Trémosa et al., 2010; Goncalves et al., 2012; Roshan et al., 2015), reported significant mass transfer associated with thermo-osmosis. Nevertheless, literatures including thermo-osmosis in coupled flow processes are limited (Zhai et al., 2020). Relevant analytical and/ numerical modelling studies include, McTigue (1986), Smith and Booker (1993), Zhou et al. (1998), Ekbote and Abousleiman (2005), Villar et al. (2005), Tong et al. (2010), Gonçalvès and Trémosa (2010), Goncalves et al. (2012), Yang et al. (2014), Roshan et al. (2015), Gao et al. (2017), Zheng et al. (2015), Salomoni (2018), Song et al. (2019), Sun et al. (2020), Zhai et al. (2020). These studies investigated the contribution of temperature driven osmotic processes on partially- or fully-coupled thermo-hydraulic-mechanical (THM) or thermo-hydraulic-chemical-mechanical (THCM) behaviours, but ignored chemical-osmosis or chemico-osmotic consolidation. Ekbote and Abousleiman (2005) developed a coupled thermo-hydraulic-chemical-mechanical model to study the thermochemical effects on borehole stability in oil and gas exploration applications. Poulet et al. (2012) also derived a coupled THCM model

to investigate the influence of folds, shear zones, and other geological structures on hydrothermal ore-deposits formation. To study the impacts of temperature on the alteration of chemical properties such as illitization of engineered barriers, Zheng et al. (2015) presented a coupled THCM model including stress balance, enthalpy balance, fluid and solute mass conservation principles. However, Ekbote and Abousleiman (2005) and Poulet et al. (2012) did not consider the influence of thermo-osmosis on solute transport. Although Zheng et al. (2015) considered the thermo-osmotic effects on solute transport, they ignored the contribution of thermal diffusion on solute transport and chemico-osmotic consolidations on the overall soil deformation. None of these models can directly calculate the soil deformation or settlement due to partial coupling or neglecting. Literatures that include both chemical-osmosis and thermo-osmosis behaviours in fully coupled THCM problems are rarely available.

In this work, the effects of both thermal and chemical osmosis on deformation and solute transport behaviours of a saturated, natural, semi-permeable clay liner are investigated. Previously presented model of Zhang et al. (2018), to study coupled hydro-mechanical-chemical behaviours of saturated natural clays including chemical-osmosis and chemico-osmotic consolidation, is extended here by including the non-isothermal flow and deformation behaviours. Unlike the previous models (Ekbote and Abousleiman, 2005; Poulet et al., 2012; Zheng et al., 2015), the presented model can directly calculate the soil settlement behaviour of semipermeable clays subjected to multiple loading mechanisms. It also includes thermal diffusion or Soret effect, and both chemico-osmotic and thermo-osmotic consolidation effects under a fully coupled modelling framework. Therefore, the presented model addresses the limitations of the previous models, and advances the knowledge and understanding of non-isothermal behaviours of semipermeable clay soils. In this paper, three loading mechanisms, namely, i) Mechanical loading, associated with a landfill-waste weight; ii) chemical loading, due to osmotic potential; and iii) thermal

loading, as a result of thermal gradient, are incorporated with simultaneous fluid, heat and solute transport mechanisms. Both molecular diffusion and thermal diffusion, and sorption processes on the solute transport behaviours are considered. The thermo-chemo-poroelastic model considers a homogenous, isotropic porous media with linear and elastic deformation. The accuracy of the model to predict non-isothermal volume change behaviours is demonstrated by validating the model against laboratory experiments obtained from the literatures. Applications of the model include a comparative analysis of the osmotic processes on soil deformation behaviour, and non-isothermal evolution of pore fluid pressure, overall settlement as well as transport and fate of a solute in a semi-permeable clay soil. The aim of this study is to present a quantitative analysis of the thermo-osmotic processes related to non-isothermal, coupled flow and deformation problems, and to investigate its relative importance on regulating volume change and solute transport behaviours when multiple loading events occur simultaneously.

2 Theoretical background

The governing equations of flow and deformation, presented here, are for one-dimensional (1D) problems. The following assumptions are made: (1) soil is homogeneous, isotropic and saturated; (2) movements occur only in the vertical direction; (3) transport of pore fluid and solutes can be explained via Darcy's law and Fick's law, respectively; and (4) the consolidation deformation of soil is linear and elastic.

2.1 Governing equations of soil deformation

The equilibrium between total stress (σ_z) and body force (f) in a small deforming soil sample is written as,

$$\frac{\partial \sigma_z}{\partial z} + f = 0 \quad (1)$$

$$f = [n\rho_f + (1-n)\rho_s]g \quad (2)$$

Where the subscript z denotes the vertical direction, n is porosity, g is the gravitational acceleration, ρ_f and ρ_s are the densities of pore fluid and soil solids, respectively. The principle of effective stress (σ_z') dictates that

$$\sigma_z' = \sigma_z - u \quad (3)$$

where u is the pore fluid pressure. Influences of three loading mechanisms, *e.g.*, mechanical, chemical and thermal loading, on the soil deformation is considered. Following (Zhang et al., 2018), the constitutive relationship of soil can be further described as,

$$\sigma_z' = \frac{E(1-\nu)}{(1-2\nu)(1+\nu)}(\varepsilon_z - \varepsilon_\pi - \varepsilon_T) \quad (4)$$

where E is the Young's modulus of elasticity, ν is Poisson's ratio, ε_z is the total strain. ε_π and ε_T represent the strains associated with chemico-osmotic consolidation and thermo-osmotic consolidation, respectively. The total strain (ε_z) is expressed in terms of soil vertical displacement (w_z) as,

$$\varepsilon_z = -\frac{\partial w_z}{\partial z} \quad (5)$$

The osmotic strain is related to the osmotic potential, *i.e.*, the osmotic suction (π), and in an incremental form it is expressed as (Barbour and Fredlund, 1989),

$$d\varepsilon_\pi = -m_\pi d\pi \quad (6)$$

where m_π is the coefficient of volume change due to the osmotic pressure gradient, and $\pi = RTc$. Here, R is the universal gas constant, T is absolute temperature in degree Kelvin and c is the solute concentration in the liquid phase. For non-isothermal condition, Eq. (6) is expanded as,

$$d\varepsilon_\pi = -m_\pi d(RTc) = -m_\pi RTdc - m_\pi RcdT. \quad (7)$$

For a thermo-elastic porous medium, the thermally induced strain is expressed after Robinet et al. (1996) as,

$$\varepsilon_T = -\alpha dT - \beta_f^T dT \tag{8}$$

where α is the thermal expansion coefficient of the soil aggregates and β_f^T is the thermal expansion coefficient of the pore fluid.

Substitution of Eqs. (2)-(8) into Eq. (1) yields,

$$\frac{E(1-\nu)}{(1+\nu)(1-2\nu)}\left[-\frac{\partial^2 w_z}{\partial z^2} + m_\pi RT\frac{\partial c}{\partial z} + \left(m_\pi Rc + \alpha + \beta_f^T\right)\frac{\partial T}{\partial z}\right] + \frac{\partial u}{\partial z} + \left[(1-n)\rho_s + n\rho_f\right]g = 0 \tag{9}$$

Eq. (9) is the governing equation of soil deformation, which includes four independent variables, *e.g.*, soil displacement (w_z), excess pore fluid pressure (u), chemical concentration (c) and temperature (T).

2.2 Governing equations of pore fluid flow

The mass conservation equation of pore fluid flow is written as (Smith, 2000),

$$\frac{\partial(\rho_f n)}{\partial t} + \nabla(\rho_f n V_f) = 0 \tag{10}$$

where V_f is the absolute velocity of the pore fluid. The Eq. (10) is expanded as,

$$\rho_f\frac{\partial n}{\partial t} + n\frac{\partial \rho_f}{\partial t} + \nabla(\rho_f n V_f) = 0. \tag{11}$$

Francois (2009) suggested that the temporal variation of pore fluid density can be expressed as a function of pore fluid pressure (u) and temperature (T). By assuming that the influence of solute concentration on pore fluid density is negligible, the temporal variation can be described as,

$$\frac{\partial \rho_f}{\partial t} = \rho_f\beta_f\frac{\partial u}{\partial t} - \rho_f\beta_f^T\frac{\partial T}{\partial t} \tag{12}$$

where β_f is the compressibility of the pore fluid.

In this study, the change in soil volume is being coupled with three loading mechanisms, *e.g.* mechanical, chemical and thermal loadings. For isothermal conditions, Kaczmarek and Hueckel (1998) proposed a relationship for porosity variation of semi-permeable clays, by incorporating mechanical

loading and chemical loading. Here, the relationship is extended by including the thermal and thermo-osmotic consolidations as,

$$n = n_0 - \Delta n = n_0 - m_v \Delta\sigma_z' - m_\pi RT\Delta c - m_\pi Rc\Delta T - \alpha\Delta T - \beta_f^T \Delta T \tag{13}$$

where m_v is the volume change coefficient related to the effective stress. The temporal derivative of Eq. (13) is expressed as,

$$\frac{\partial n}{\partial t} = m_v \frac{\partial u}{\partial t} - m_\pi RT \frac{\partial c}{\partial t} - \left(m_\pi Rc + \alpha + \beta_f^T\right)\frac{\partial T}{\partial t} \tag{14}$$

The absolute pore fluid velocity (V_f) combines the pore fluid relative velocity with respect to the soil skeleton (V_r) and the absolute velocity of the soil-skeleton deformation (V_s) as,

$$V_f = V_r + V_s \tag{15}$$

$$V_r = \frac{1}{n} V \tag{15a}$$

$$V_s = \frac{\partial w_z}{\partial t} \tag{15b}$$

where V is the velocity of the pore fluid flow and it combines the contributions of hydraulic head, osmotic-pressure head and temperature gradients. Gonçalvès and Trémosa (2010) explained the thermo-osmotically driven pore fluid flow as,

$$V_T = \frac{k_T}{\mu_{l(T)}} \frac{\partial T}{\partial z} \tag{16}$$

where V_T is the pore fluid velocity associated with the temperature gradient and k_T is the thermo-osmotic conductivity. $\mu_{l(T)}$is the temperature-dependent dynamic viscosity of water.

Fluid flow due to hydraulic head gradient (V_u) and osmotic-pressure head gradient (V_π) are presented in Smith (2000) and Zhang et al. (2018). Here, the relationship is extended by including V_T as,

$$V = V_u + V_\pi + V_T = -\frac{k_h}{\gamma_w}\frac{\partial u}{\partial z} + \omega \frac{RT}{M}\frac{k_h}{\gamma_w}\frac{\partial c}{\partial z} + \frac{k_T}{\mu_l}\frac{\partial T}{\partial z} \tag{17}$$

where k_h is *in-situ* hydraulic conductivity, $\gamma_w$is the unit weight of water, M is the molar mass, and ω is the osmotic efficiency. Here, $\omega \frac{RT}{M}\frac{k_h}{\gamma_w} = k_\omega$, *i.e.*, the osmotic conductivity. Hart and John (1986)

described the in-situ hydraulic conductivity (k_h) in terms of initial hydraulic conductivity (k_{h0}) and initial porosity (n_0) as,

$$k_h = k_{h0}\left(\frac{n}{n_0}\right)^3 \tag{18}$$

Substituting Eqs. (12), (14) and (17) into Eq. (11) yields the governing equation of pore fluid flow,

$$\left(m_v + n\beta_f\right)\frac{\partial u}{\partial t} - m_\pi RT\frac{\partial c}{\partial t} - \left(m_\pi Rc + \alpha + n\beta_f^T\right)\frac{\partial T}{\partial t} = -\frac{\partial}{\partial z}\left[-\frac{k_h}{\gamma_w}\frac{\partial u}{\partial z} + \frac{RT}{M}\frac{k_c}{\gamma_w}\frac{\partial c}{\partial z} + \frac{k_T}{\mu_l}\frac{\partial T}{\partial z} - n\frac{\partial w_z}{\partial t}\right] \tag{19}$$

2.3 Governing equations of heat transfer

Following the energy conservation law heat transport in soil, in absence of a source/sink, is written as,

$$\frac{\partial \Phi}{\partial t} = -\frac{\partial Q}{\partial z} \tag{20}$$

where Q is the heat flux per unit volume of soil and Φ is the heat content. Considering that the different components of the soil are in thermal equilibrium, heat content is expressed as (Thomas and Cleall, 1999),

$$\Phi = [(1-n)C_{ps}\rho_s + nC_{pf}\rho_f](T - T_r) \tag{21}$$

where C_{ps} and C_{pf} are the specific heat capacity of the solid particles and pore liquid, respectively, and T_r is the reference temperature.

We consider two modes of heat transfer in soil, *e.g.*, thermal conduction and convection. The heat flux is therefore expressed as,

$$Q = -\lambda_T\frac{\partial T}{\partial z} + C_{pf}\rho_f V(T - T_r) \tag{22}$$

where λ_T is the intrinsic thermal conductivity of the soil.

Substitution of Eqs. (21)-(22) into Eq. (20) yields the governing heat transfer equation as

$$A\frac{\partial T}{\partial t} + B\frac{\partial u}{\partial t} + C\frac{\partial c}{\partial t} = -\frac{\partial}{\partial z}\left[-\lambda_T\frac{\partial T}{\partial z} + C_{pf}\rho_f(T - T_r)\left(-\frac{k_h}{\gamma_w}\frac{\partial u}{\partial z} + \omega\frac{RT}{M}\frac{k_h}{\gamma_w}\frac{\partial c}{\partial z} + \frac{k_T}{\mu_l}\frac{\partial T}{\partial z}\right)\right] \tag{23}$$

$$A = C_{ps}\rho_s + [n - (T - T_r)(m_\pi Rc + \alpha)]\left(C_{pf}\rho_f - C_{ps}\rho_s\right) - (T - T_r)nC_{pf}\rho_f\beta_f^T \quad (23a)$$

$$B = (T - T_r)\left(C_{pf}\rho_f m_v - C_{ps}\rho_s m_v + nC_{pf}\beta_f\right) \quad (23b)$$

$$C = (T - T_r)\left(C_{pf}\rho_f - C_{ps}\rho_s\right)m_\pi RT \quad (23c)$$

194

195 ***2.4 Governing equations of solute transport***

196 Transport of a solute in pore fluid is explained as,

$$\frac{\partial(nc)}{\partial t} = -\frac{J_f}{\partial z} \pm Y \quad (24)$$

197 where J_f is the total solute flux in the pore fluid, and Y is the sink/source term. The total flux combines

198 convection, molecular diffusion and thermal diffusion and it is expressed as,

$$J_f = J_c + J_{D_c} + J_{D_T} \quad (25)$$

199 where J_c, J_{D_c}, and J_{D_T} represent solute flux due to convection, molecular diffusion and thermal

200 diffusion, respectively. They are defined as,

$$J_c = cV = c\left((1-\omega)\left(-\frac{k_h}{\gamma_w}\frac{\partial u}{\partial z}\right) + \omega\frac{k_h}{\gamma_w}\frac{RT}{M}\frac{\partial c}{\partial z} + \frac{k_T}{\mu_l}\frac{\partial T}{\partial z}\right) \quad (26)$$

$$J_{D_c} = -nD_c\frac{\partial c}{\partial z} \quad (27)$$

$$J_{D_T} = -n\tau D_0 S_T c\frac{\partial T}{\partial z} \quad (28)$$

201 where D_c is the effective diffusion coefficient, D_0 is the diffusion coefficient of the solute in free liquid.

202 Eq. (28) calculates the contribution of temperature on the solute diffusion, *i.e.*, the Soret effect, and S_T

203 is the Soret coefficient. τ is the tortuosity factor and it lies between $0 < \tau < 1$. In this work, τ is

204 calculated following Liu et al. (2004) as,

$$\tau = n^2 \quad (29)$$

205 Malusis et al. (2015) described the effective diffusion coefficient of semipermeable clays as,

$$D_c = \tau(1-\omega)D_0 \tag{30}$$

206 Substitution of Eqs. (25)-(30) into Eq. (24) yields

$$\frac{\partial(nc)}{\partial t} = -\frac{\partial}{\partial z}\left((1-\omega)\left(-\frac{k_h}{\gamma_w}\frac{\partial u}{\partial z}\right)c + \omega\frac{RT}{M}\frac{k_h}{\gamma_w}\frac{\partial c}{\partial z}c + \frac{k_T}{\mu_l}\frac{\partial T}{\partial z}c - nD_c\frac{\partial c}{\partial z} - n\tau D_0 S_T c\frac{\partial T}{\partial z}\right) \pm Y \tag{31}$$

207 Eq. (31) is the governing equation of solute transport in the pore fluid.

208 The mass conservation equation of a solute adsorbed in soil aggregates is written as,

$$\frac{\partial[(1-n)\rho_s S]}{\partial t} = -\frac{\partial J_s}{\partial z} \pm Y \tag{32}$$

209 where S represents the amount of solute adsorbed in the solid phase. J_s is the solute flux in the solid

210 phase, which is expressed as,

$$J_s = (1-n)V_s\rho_s S. \tag{33}$$

211 Here, solid-solution partitioning is descried as,

$$S = K_d c \tag{34}$$

212 where K_d is the partitioning or distribution coefficient.

213 Substitution of Eqs. (33)-(34) into Eq. (32) yields

$$\frac{\partial[(1-n)\rho_s K_d c]}{\partial t} = -\frac{\partial}{\partial z}\left[(1-n)\frac{\partial w_z}{\partial t}\rho_s K_d c\right] \pm Y \tag{35}$$

214 which is the governing equation of solute transport in the solid phase.

215 According to the mass balance of solute, combining Eq. (31) and (35) together, then

$$\frac{\partial(nc)}{\partial t} + \frac{\partial[(1-n)\rho_s K_d c]}{\partial t} = -\frac{\partial}{\partial z}\left((1-\omega)\left(-\frac{k_h}{\gamma_w}\frac{\partial u}{\partial z}\right)c + \omega\frac{RT}{M}\frac{k_h}{\gamma_w}\frac{\partial c}{\partial z}c + \frac{k_T}{\mu_l}\frac{\partial T}{\partial z}c - nD_c\frac{\partial c}{\partial z} - n\tau D_0 S_T c\frac{\partial T}{\partial z}\right) - \frac{\partial}{\partial z}\left[(1-n)\frac{\partial w_z}{\partial t}\rho_s K_d c\right] \tag{36}$$

216 Eq. (36) is the final governing equation of solute transport in a porous medium.

217

218 **3. Model validation**

Partial validation of the model is presented in this section. Full model validation could not be performed due to lack of experimental data. The accuracy of the model on predicting thermo-osmosis and the influence of thermal gradient on solute transport has been tested here by comparing with relevant experimental data obtained from the literature. More validation and/ verification of the model, especially the chemical-osmosis processes are presented in Zhang et al. (2018). The model simulations have been carried out using the COMSOL Multiphysics (https://www.comsol.com) software.

3.1 Comparison with the results of Delage et al. (2000)

Delage et al. (2000) conducted experimental investigation on temperature induced volume change of clay-water system and subsequent consolidation in saturated Boom clays. Samples (76 mm height and 38 mm diameter) were tested in a triaxial compression cell under a constant isotropic stress of 4 MPa and temperatures up to 100°C. Thermal dilation and expulsion of porewater from the samples during the drained consolidation tests allowed the thermo-osmotic consolidation to take place. Here the model predicted results have been compared with the thermal volume change behaviour of the clay-water system observed in their experiment. To account thermal dilation, Baldi et al. (1988) expressed the porewater thermal expansion coefficient (β_f^T) as a function of temperature and water pressure as,

$$\beta_f^T(T,u) = \alpha_0 + (\alpha_1 + \beta_1 T)\ln(mu) + (\alpha_2 + \beta_2 T)\big(\ln(mu)\big)^2 \quad (37)$$

where α_0(=4.505×10^{-4} °C^{-1}), α_1(=9.156×10^{-5} °C^{-1}), α_2(=6.381×10^{-6} °C^{-1}), β_1(= -1.2×10^{-6} °C^{-2}), β_2(= -5.766×10^{-8} °C^{-2}), m(=15 MPa^{-1}) are constants.

Table 1 Parameters used to compare simulation results against the result of Delage et al. (2000)

Parameters	Values	References

Initial porosity, n_0	0.370	
Initial hydraulic conductivity, k_{h0}	2.0×10^{-12} ms^{-1}	Delage et al. (2000)
Coefficient of volume change, m_v	1×10^{-5} Pa^{-1}	Delage et al. (2000)
Unit weight of liquid, γ_w	10 kNm^{-3}	
Density of the soil, ρ_s	2600 kgm^{-3}	
Modulus of elasticity, $\boldsymbol{E}$	200 MPa	Francois et al. (2009)
Poisson's ratio, $\boldsymbol{\nu}$	0.3	Peters and Smith (2004)
Thermal expansion coefficient of soil, α	1×10^{-5} °C^{-1}	Delage et al. (2000)
Compressibility of pore liquid, β_f,	4.5×10^{-10} Pa^{-1}	Francois et al. (2009)
Specific heat capacity of soil, $\boldsymbol{C_{ps}}$	2.85×10^{6} Jm^{-3}K^{-1}	Delage et al. (2000)
Specific heat capacity of pore liquid, C_{pf}	4186 Jkg^{-1}K^{-1}	Francois et al. (2009)
Intrinsic thermal conductivity of soil, λ_T	1.7 Wm^{-1}K^{-1}	Delage et al. (2000)

The parameters used in the validation exercise are listed in Table 1. The initial temperature $T(z,0)$ = 293 K, ($0 \leq z < L$ and L =0.076 m), while the boundary temperature $T(L,t)$= 373 K ($t \geq 0$). The porewater pressure remained constant throughout the simulation, i.e. $u(z,t)$= 4 MPa, ($0 \leq z \leq L$ and $t \geq 0$) The simulation time (t) is 266.67 h.

The results are presented in Fig.1. The model predicted result shows good agreement with the experimental result. Temperature induced porewater expansion and expulsion caused the sample to contract and, therefore, reduced its porosity. The decreased volume or porosity reduction is associated with the dissipation of porewater pressure. Delage et al. (2000) conducted four tests using the same sample. Here we compared the 'Test 1' results which was suggested as better quality than the other test

results (that exhibited anomalies at lower temperature regimes). The deviation observed at higher temperatures (70-100°C), where the model under-estimated the rate of porosity reduction (or porewater pressure dissipation), may be due to the uncertainties associated with the additional model parameters used in the simulation.

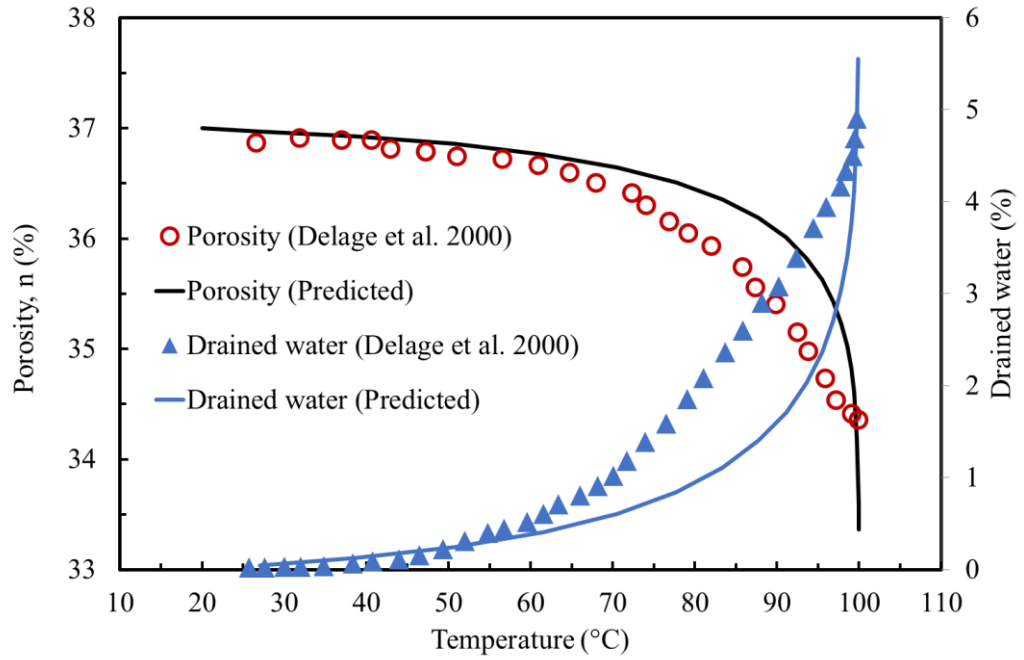

a)

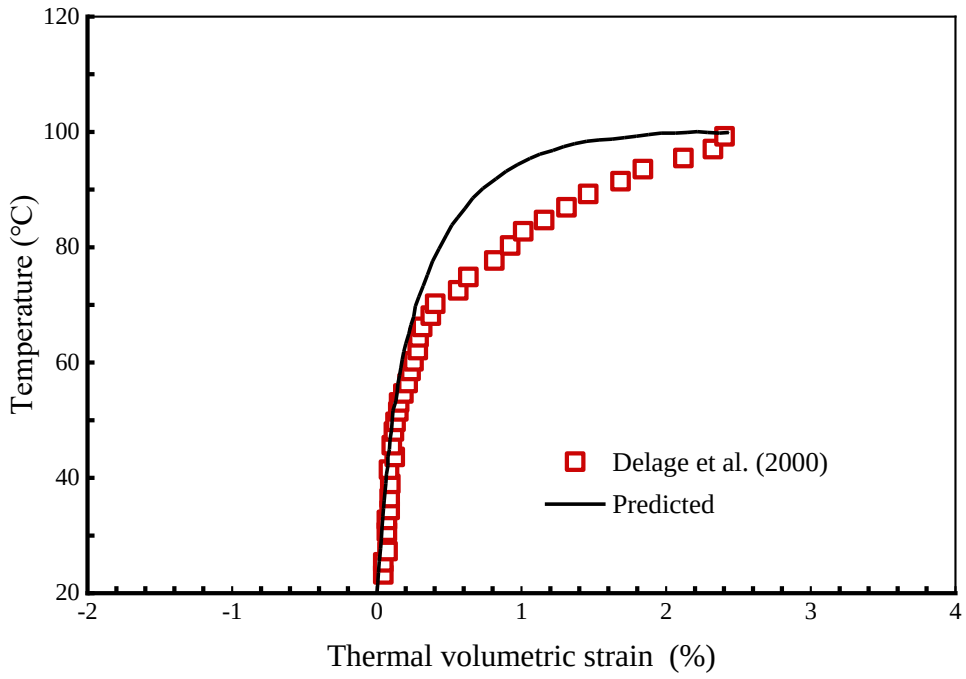

b)

Figure 1 Comparison of model predicted result of temperature induced (a) porosity and drained water variation and (b) thermal volumetric strain with that of the Delage et al. (2000).

3.2 Comparison with the results of Do et al. (2006)

Do et al. (2006) investigated effects of temperature on zinc (Zn^{2+}) and cadmium (Cd^{2+}) diffusion in natural clays collected from southwester Korea. Laboratory soil column tests were conducted at various temperatures ranging from 15°C to 55°C. Here, the results are compared with the experiments conducted at 55°C. 100 mm by 50 mm solute free clay samples were exposed, individually, to a source concentration of 500 mg L^{-1} $Zn^{2+}$and 300 mg L^{-1} Cd^{2+} and their transport in the soil columns were observed for 30 days.

Table 2 Simulation conditions to test against the results of Do et al. (2006)

Initial conditions	$c(z,0) = 0$	$T(z,0)$ =273 K	$(0 < z < L)$
Boundary conditions	$c(0,t) = c_0$	$T(0,t) = 328$ K	$(t \geq 0)$
	$\frac{\partial c}{\partial x}(L,t) = 0$	$T(L,t) =$ 273 K	$(t \geq 0)$

Table 3 Parameters used to compare simulation results against the result of Do et al. (2006)

Parameters	**Values**	**References**
Porosity, *n*	0.43	Do et al. (2006)
Molar mass of Zn^{2+}	0.065 kg m^{-3}	
Molar mass of Cd^{2+}	0.112 kg m^{-3}	

Soret Coefficient, $\boldsymbol{S_T}$	0.033 K^{-1}	Hart and John (1986)
Diffusion coefficient (D_0) of Zn^{2+}	7.02×10^{-10} m^2 s^{-1}	Lide (1997)
Diffusion coefficient (D_0) of Cd^{2+}	7.17×10^{-10} m^2 s^{-1}	Lide (1997)
Distribution coefficient K_d of Zn^{2+}	12.1 L kg^{-1}	Lin (2008)
Distribution coefficient K_d of Cd^{2+}	26.8 L kg^{-1}	Lin (2008)

The initial and boundary conditions of the simulation are presented in Table 2 and the parameters in Table 3. The simulation results and their comparison with that of Do et al. (2006) are presented in Fig.2. It is obvious from the graphs that the model predicted results agree well with the results of Do et al. (2006). The transport of Zn^{2+} and Cd^{2+} in these results are influenced by both the concentration gradients and the thermally induced diffusion or the Soret effect. The results also highlight accurate implementation of the mechanisms and its accuracy of prediction.

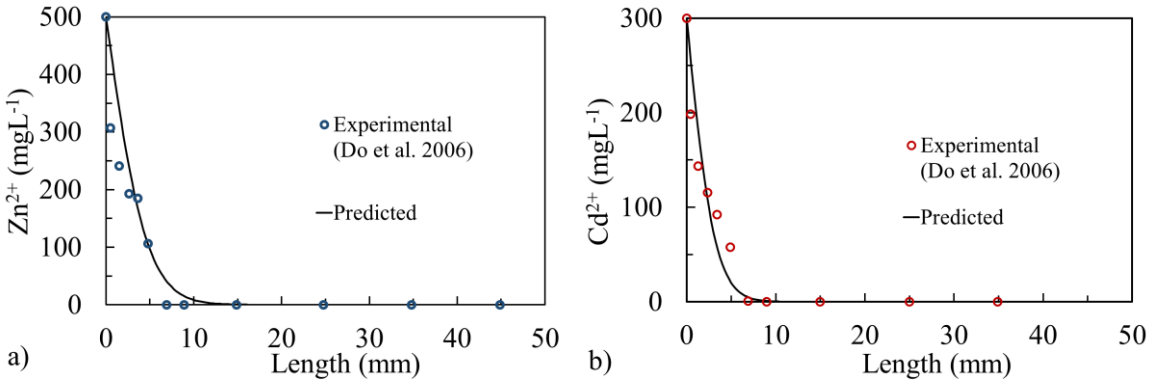

Figure 2 Comparison of model predicted concentration profiles of a) Zn^{2+} and b) Cd^{2+} against the results of Do et al. (2006).

4. Model applications

The model applications presented in this section investigate the relative importance of osmotic processes on non-isothermal coupled flow and deformation behaviour of a semi-permeable clay liner (bentonite) used in a generic landfill site.

4.1 Problem description

Waste weight and waste degradation, temperature evolution, leachate formation, and seepage create a complex, challenging scenario, for which optimum performance of the clay liner should be ensured and maintained to restrict the movement or spread of contaminants. Here, the model is used to simulate a number of coupled landfill processes in a 1D clay liner domain. Transport of a representative trace metal, e.g., Cadmium, is predicted in the saturated clay liner subjected to simultaneous thermal, chemical and mechanical loading events. Cadmium is a toxic heavy metal and causes adverse health consequences in human and animals when ingested at higher dosage.

Chen et al. (2015, 2016) reported that biological degradation of landfill waste can elevates the temperature at the top of the liner up to 80°C or 353 K, while the bottom temperature remains 20°C or 293 K. This creates a temperature gradient of 60°C across a 1.0 m long clay liner. In the simulations, three different temperatures, e.g. 313 K, 333 K and 353 K, have been considered at the top, while 293 K at the bottom, yielding ΔT = 20, 40 and 60, respectively. The simulation period is up to 100 years. The initial and boundary conditions of the simulations are presented in Table 4.

Table 4 Initial and boundary conditions to investigate coupled THCM behaviour of a natural clay liner

Initial conditions	Boundary conditions	
$(0 < z < L)$	$(t > 0)$	
$w(z, 0) = 0$	-	$w(L, t) = 0$

$u(z, 0) = P$ =50 kPa	$u(0, t)$= 0	$u(L, t)$= 0
$c(z, 0)$=0	$c(0, t)$= 225	$c(L, t)$= 0
$T(z, 0)$=*293K*	$T(0, t)$= 313K/333K/353K	T(L, t)= 293K

301

302 **4.2 Model parameters**

303 The model parameters are listed in Table 5. Gonçalvès and Trémosa (2010) compiled a list of thermo-
304 osmotic conductivity data, from literatures, for various clays and expressed them in "$m^2\,K^{-1}\,s^{-1}$" unit by
305 implicitly accounting the dynamic viscosity of water and osmotic efficiency of clayey soils. However, in
306 these simulations the thermo-osmotic conductivity (k_T) is calculated following Gonçalvès et al. (2012).
307 This is because under non-isothermal condition μ_l is a function of temperature (T) and by considering
308 it implicitly in $m^2\,K^{-1}\,s^{-1}$ units will undermine the important thermo-physical property of clay-water
309 system. For boom clay, they reported the ratio of k_T/k in the range 2.5 - 250 Pa K^{-1}, where the intrinsic
310 permeability $k = 5.0\times10^{-18}\,m^2$. For k_T/k = 6.5 Pa K^{-1}, the value of $k_T = 3.25\times10^{-17}$ Pa $m^2\,K^{-1}$ or 3.25×10^{-17}
311 N K^{-1}.

312

313 The temperature-dependent viscosity $\mu_{l(T)}$ is estimated following (Kaye and Laby, 1986) as,

$$\mu_{l(T)} = 661.2\,(T - 229)^{-1.562} \times 10^{-3} \pm 0.5\% \quad (38)$$

314 **Table 5** Model parameters for the long-term simulation/ model application

Parameters	Values	References
Initial porosity, n_0	0.5	
Molar mass of NaCl, M	0.112 kg mol^{-1}	

Osmotic efficiency, ω	0.005	Huang et al. (2015)
Density of the solid soil, ρ_s	2600 kg m^{-3}	Gonçalvès et al. (2012)
Diffusion coefficient (D_0) of Cd^{2+}	3.837×10^{-9} m^2 s^{-1}	Araujo et al. (2007)
Initial hydraulic conductivity, k_0	1.0×10^{-10} m s^{-1}	Kaczmarek et al. (1997)
Poisson's ratio, v	0.3	Peters and Smith (2004)
Modulus of elasticity, E	1.49×10^{6} Pa^{-1}	Zhang et al. (2018)
Universal gas constant, R	8.314 J mol^{-1} K^{-1}	
Unit weight of the pore water, γ_w	10 kN m^{-3}	
Distribution coefficient, k_d	14.3×10^{-3} m^3 kg^{-1}	Lin (2008)
Coefficient of volume change, m_v	5×10^{-7} Pa^{-1}	Delage et al. (2000)
Coefficient of volume change, $\boldsymbol{m_\pi}$	0.105×10^{-7} Pa^{-1}	Kaczmarek and Hueckel (1998)
Soret coefficient, S_T,	0.033 K^{-1}	Hart and John (1986)
Thermo-osmotic conductivity, k_T	3.25×10^{-17} Pa m^2 K^{-1}	Gonçalvès et al. (2012)
Thermal expansion coefficient, α	2.4×10^{-4} K^{-1}	Hong et al. (2013)
Compressibility of pore fluid, β_f,	4.5×10^{-10} Pa^{-1}	Francois et al. (2009)
Pore fluid thermal coefficient, β_f^T	3.5×10^{-4} K^{-1}	Francois et al. (2009)
Specific heat capacity, C_{ps}	732 J kg^{-1} K^{-1}	Francois et al. (2009)
Specific heat capacity, C_{pf}	4186 J kg^{-1} K^{-1}	Francois et al. (2009)
Thermal conductivity of soil, λ_T	1.69 W m^{-1} K^{-1}	Francois et al. (2009)

5. Results and Discussion

5.1 Effect of osmosis on the overall consolidation behaviour

318 The contributions of osmotic processes on the clay liner deformation are presented here. Various
319 loading conditions including chemical-osmosis and thermo-osmosis are included in non-isothermal
320 coupled flow simulations to estimate their relative dominance on the liner deformation. The results of
321 four loading conditions, namely, Case 1: mechanical loading only; Case 2: mechanical loading and
322 chemical-osmosis; Case 3: mechanical loading and thermo-osmosis; and Case 4: mechanical loading,
323 chemical-osmosis and thermo-osmosis, at the source temperature of 333 K are presented in Fig.3. The
324 deformation behaviour is explained by analysing the change in void ratio of the clay liner.

325 Fig.3a and 3b show the evolution of void ratio respectively at z = 0.25 m and 0.50 m for the four
326 loading cases. In both figures, the lowest volume change is observed when the deformation is solely
327 controlled by the mechanical loading, i.e. Case 1. The combination of mechanical loading, thermo-
328 osmosis and chemical-osmosis (Case 4) results into the maximum deformation of the liner. The minimum
329 void ratio observed in Fig.3a Case 1 and Case 4 are 0.94 and 0.86, while in Fig.3b these are 0.94 and 0.88,
330 respectively. For the given simulation conditions and parameter regime, this represents an additional
331 reduction of 8%, at 0.25 m depth, and 6%, at 0.50 m, of overall soil volume in Case 4 than in Case 1. In
332 the simulation, liner temperature elevates rapidly and reaches to the applied temperature of 333 K at the
333 boundary. The graphs of Case 3 as well Case 4, in both figures, indicate expansion of the clay liner during
334 the temperature growth period (until around 0.01 years). This is related to the thermally induced
335 expansions of soil skeleton and the pore fluid volume.

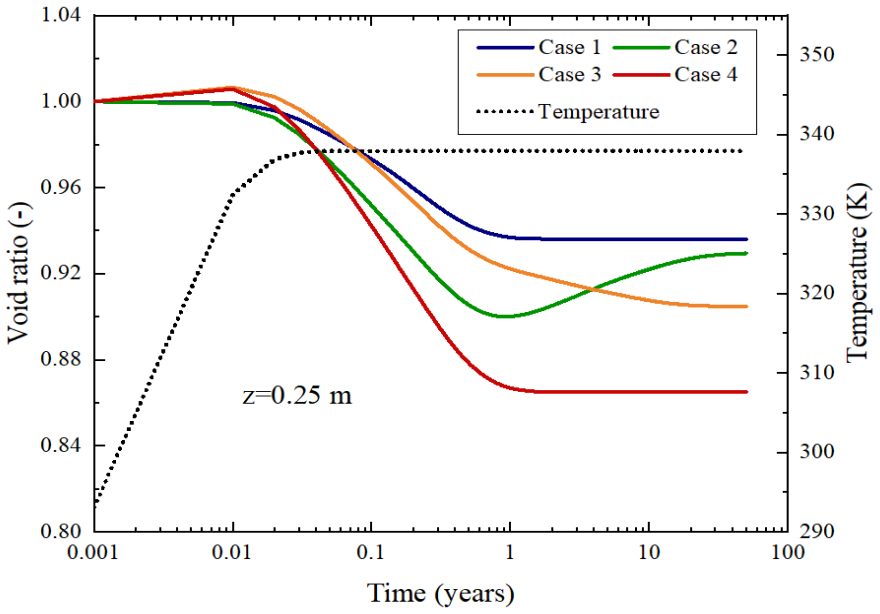

a)

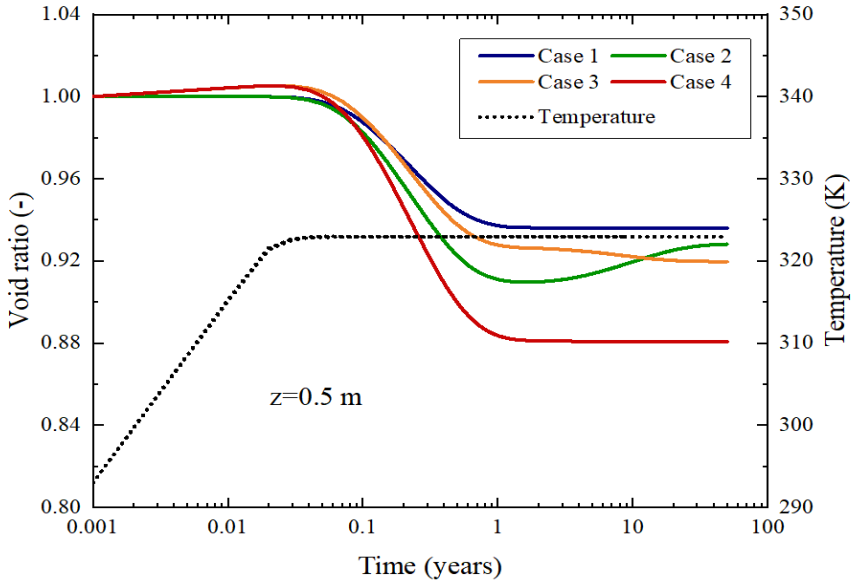

b)

Figure 3 Evolution of void ratio and temperature at a) 0.25 m and b) 0.50 m depth of the semi-permeable clay liner for various loading situations. Case 1: mechanical loading only; Case 2: mechanical loading and chemical-osmosis; Case 3: mechanical loading and thermo-osmosis; and Case 4: mechanical loading, chemical-osmosis, and thermo-osmosis effects.

Following the initial expansion, pore fluid expulsion, assisted by the thermo-osmotic conductivity of the clay liner, occurs through the drainage boundary and causes thermo-osmotic consolidation. Closer

to the heat source the effect of thermo-osmotic consolidation and thermal consolidation is larger, which reduces gradually with the distance. This is noticeable, since the predicted slopes of Case 3 graphs in Fig.3a are steeper than that of Fig.3b.

The Case 2 graphs, which include the combined effects of mechanical loading and chemical-osmosis, show that initially the overall deformation is dominated by mechanical consolidation and in the long term chemico-osmotic consolidation becomes more prevalent. With time the gradient of solute concentration or chemical potential across the clay liner decreases and subsequently the effect of chemico-osmotic consolidation, which explains the 'rebound shape' observed in the Case 2 results. A detailed study on chemical-osmosis and chemico-osmotic consolidation behaviour of semi-permeable clays are presented in Zhang et al. (2018). It should be noted that under non-isothermal conditions temperature variations also influence the chemico-osmotic consolidation behaviours (as per Eq. (7)).

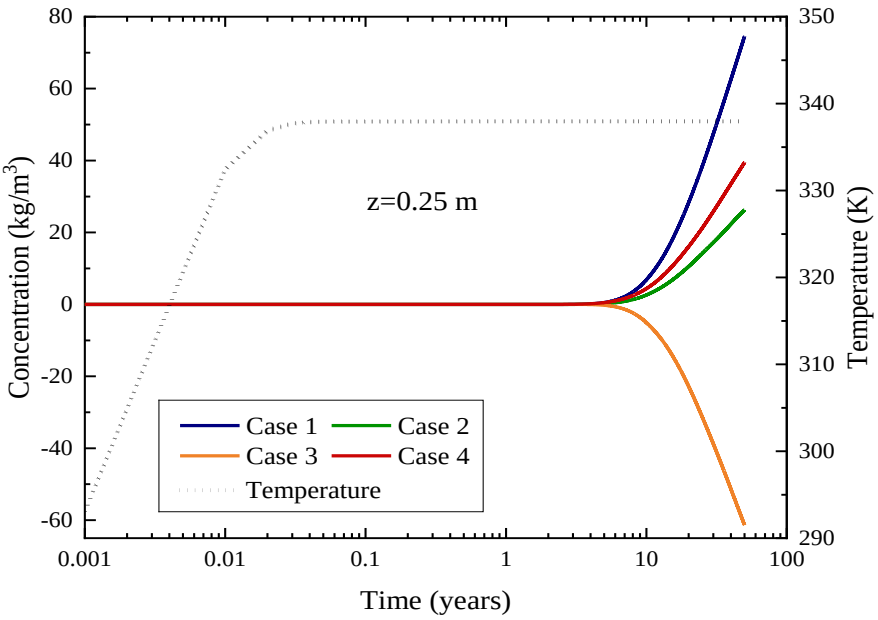

a)

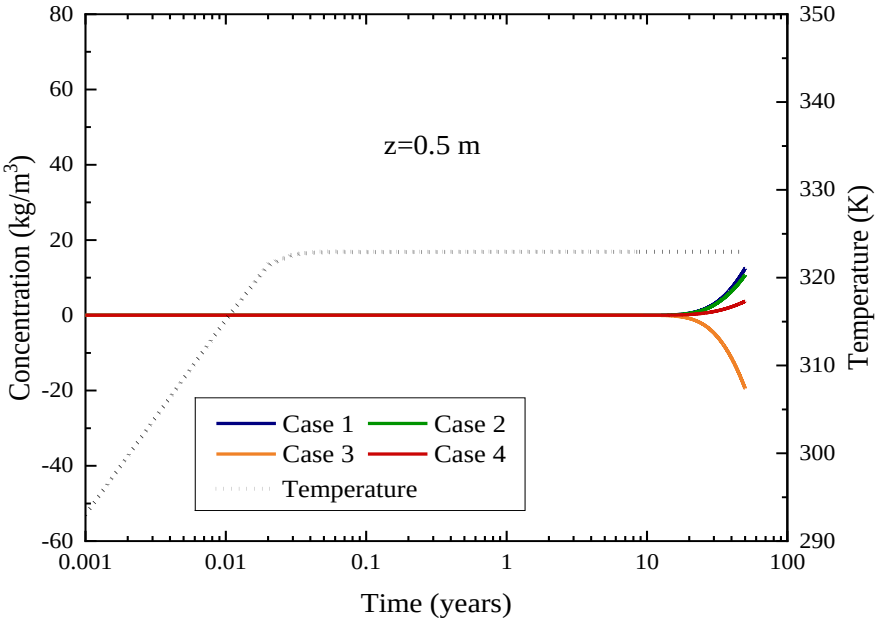

b)

Figure 4 Evolution of solute concentration and temperature at (a) 0.25 m and (b) 0.50 m depth of the semi-permeable clay liner for various solute transport mechanisms. Case 1: chemical diffusion only; Case 2: thermal diffusion only; Case 3: fluid diffusion only; and Case 4: fluid diffusion, thermal diffusion, and chemical diffusion.

The calculated characteristic time $\left(\approx {}^{L^2}/_{D_c}\right)$for cadmium diffusion, for the parameter regime, are 2.05 years and 8.2 years at 0.25 m and 0.5 m, respectively. This is also noticeable in Figure 4a and 4b, which show the calculated results for the fluid diffusion, thermal diffusion, and chemical diffusion and combined actions in this consolidation problem. In comparison the characteristic times of thermal diffusivity, which is the ratio between thermal conductivity and specific heat capacity ($\approx 1.77 \times 10^{-6}$ m^2/s), for the corresponding characteristics length are significantly shorter, *e.g.*, 9.8 hours and 39.2 hours. Based on the calculated coefficient of consolidation of 2.04×10^{-8} m^2/s, the corresponding characteristic times for fluid diffusion are 35.4 days and 138.7 days. Therefore, the simulations suggest that the heat equilibrium reaches faster and before the pore water expulsion. The concentration equilibrium occurs at last. This means that the effects of heat transfer, fluid dissipation, and solute transport on the overall consolidation

373 of the liner occur perhaps independently.

374

375 ***5.2 Influence of temperature on the evolution and distribution of pore water***

376 The evolution of excess pore water pressure along the depth of the clay liner is presented in Fig.5
377 for various temperature regimes. The results show that during the early simulation period (0.1 year),
378 excess pore water pressure is positive and reaches near the applied mechanical pressure of 50 kPa. The
379 positive porewater pressure (or compression) is associated with the mechanical consolidation and it
380 increases further with temperature. This effect of temperature is repeated in each pressure profiles drawn
381 at the individual simulation times, *i.e.* t = 0.1, 1.0 etc. However, the excess positive pressure disappears
382 rapidly and leads to negative pressure development. The negative pressure in the clay liner occurs due to
383 concurrent influence of chemical-osmosis and thermo-osmosis which expel pore water from the liner and
384 results into negative pore water pressures. Therefore, under non-isothermal conditions, excess pore water
385 pressure in semi-permeable clays is initially influenced by the mechanical loading and later combinedly
386 by the osmotic loadings. The effects of osmotic consolidations on the excess pore wate pressure gradually
387 diminishes since both solute-concentration-gradient and temperature-gradient across semi-permeable
388 clay membranes reduces with time.

389

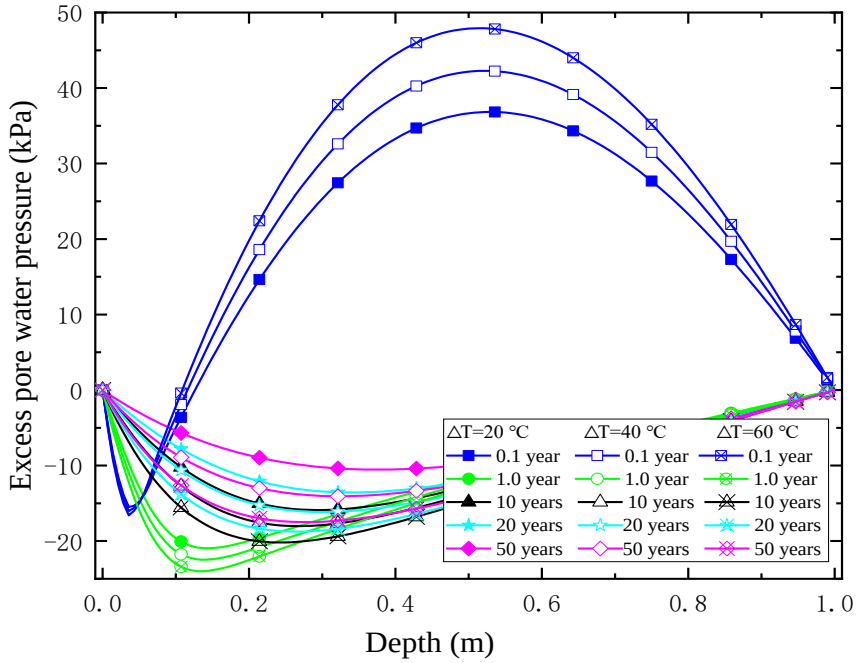

390

391 **Figure 5** Evolution and distribution of excess pore water pressure in the semi-permeable clay liner.

392

393 ***5.3 Influence of temperature on the overall liner settlement***

394 The results of time-dependent settlement behaviour of the clay liner are presented Fig.6. The graphs

395 plotted for the individual source temperatures exhibit an initial (I) increasing phase, followed by a (II)

396 decreasing phase.

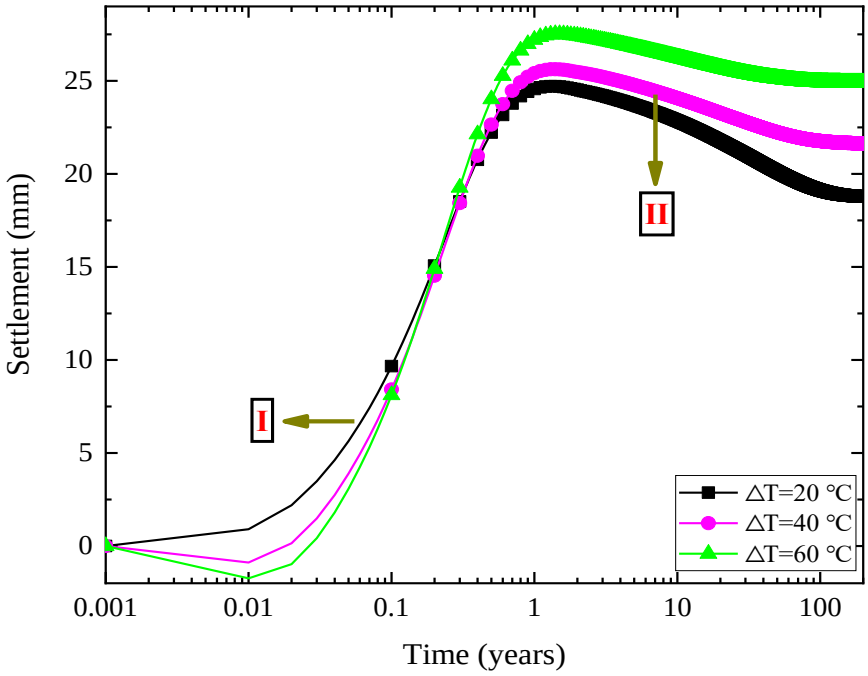

Figure 6 Evolution of the clay liner settlement for various temperature regimes.

At lower temperatures, e.g. ΔT = 20°C, the contribution of thermally induced consolidation or expansion on the overall settlement is smaller and the settlement is dominated by the mechanical loading. The contributions of thermal volume change on the settlement increases with temperature, e.g. ΔT = 40°C or 60°C. The graphs at these temperature regimes show an initial expansion of the liner that is due to the thermal dilation of the solid phase and the liquid phase. However, the differential expansion of the phases (liquid dilation is usually larger than a solid at a given temperature) leads to expulsion of pore water across the semi-permeable clay membrane under the drained boundary condition, i.e., thermo-osmotic consolidation. At higher temperature, the influence of thermo-osmotic consolidation on the overall settlement behaviour therefore increases. The peak settlement also increases with temperature. The maximum settlement of 27.55 mm is calculated at 353 K (or ΔT = 60°C), which is an increase of 11.3% from the peak settlement of 24.71 mm at the 313 K (or ΔT = 20°C). It is shown in Fig.3 that the mechanical consolidation occurs relatively fast and in the long-term both thermo-osmosis and chemical osmosis

influence the settlement behaviour. As the elevated thermo-osmotic-gradient and chemical-osmotic-gradient diminishes with time, the direction of pore water flow across the semi-permeable membrane reverses which leads to continuous reduction of the liner settlement. This explains the rebound shape observed in the phase II of Fig.6.

5.4 Influence of temperature and osmotic processes on the overall solute transport behaviour

The solute transport results in the clay liner is presented in Fig.7. In the simulations, a number of processes and their coupled interactions, including Fickian diffusion, temperature-induced diffusion or Soret effect, osmotically driven advection, chemico-osmotic consolidation, thermo-osmotic consolidation, mechanical consolidation and solid-solution partitioning or sorption, regulated the solute spread in the model domain. The results show that in semi-permeable clays solute spread is affected negatively with temperature, despite the influence of temperature on the solute movement (or the Soret effect) is positive. It is shown in Fig.6 that the liner settlement increases with temperature. That means that the solute transport is retarded further in a more compacted clay liner and, therefore, the effect of thermo-osmotic consolidation on the solute transport dominates over Soret diffusion. After 50 years, the concentration of 100 kg/m^3 Cd^{2+} is predicted up to 0.12 m, 0.20 m, and 0.28 m depth, for ΔT = 20, 40, 60°C, respectively. For a 20°C increase in temperature the spread of cadmium in the liner is reduced by 8 cm for the current parameter regimes and the simulation conditions.

In practice, such as, landfill operations that often use clayey soils as barrier materials and where heat generation is significant, the effects of thermally driven consolidations should not be ignored, since it may significantly deviate the predicted outcomes. To highlight the importance of thermo-osmotic consolidation on solute transport, a comparison between hydro-mechanical-chemical (HMC) behaviour

434 and thermo-hydro-mechanical-chemical (THMC) behaviour of the clay liner is presented in Fig.8.

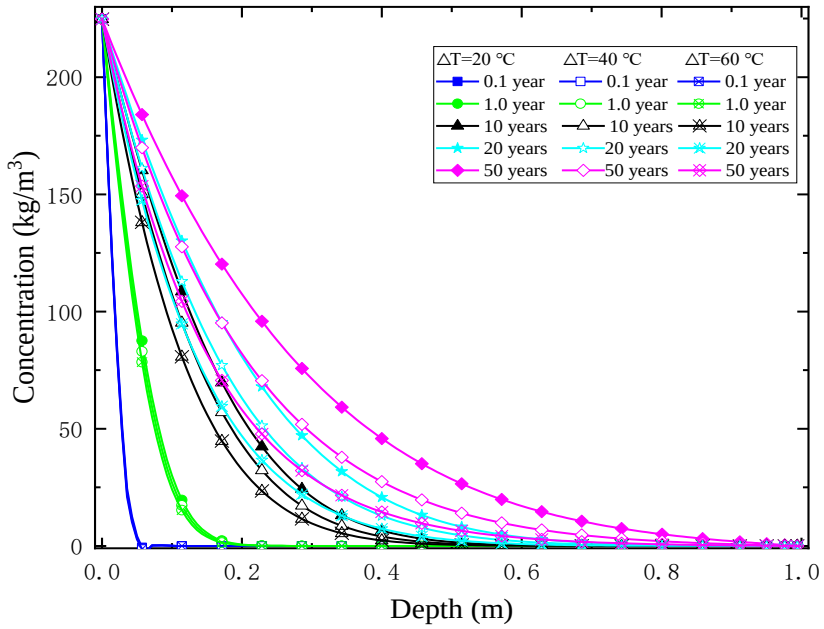

435

436 **Figure 7** Evolution of solute concentrations along the depth of the liner for various temperatures.

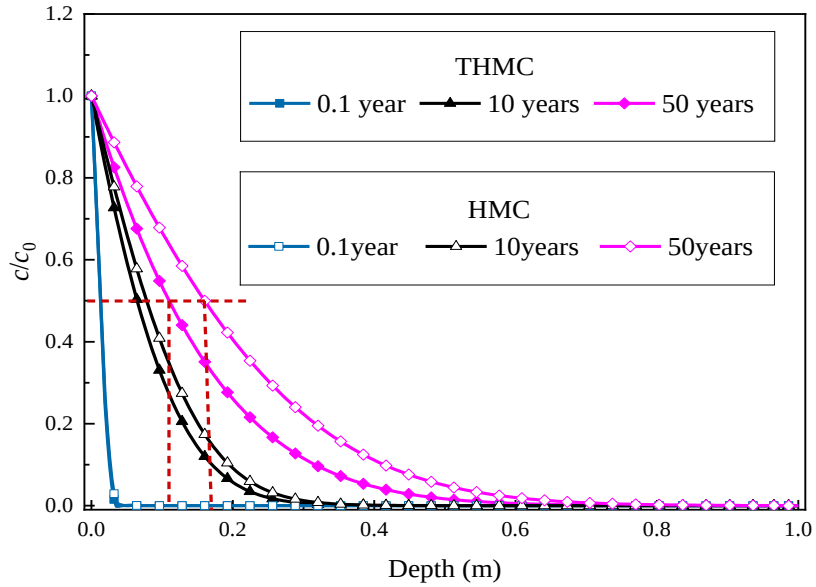

437

438 **Figure 8** Effect of temperature on solute transport behaviour in a saturated, semi-permeable clay liner.

439 THMC represents thermo-hydro-mechanical-chemical behaviour for non-isothermal simulation, whereas,

440 HMC represent hydro-mechanical-chemical behaviour during isothermal simulations.

441

442 From the results of Fig.8, it is evident that significant difference exists between the THMC and the

443 HMC simulation. The solute concentration values in THMC simulations are less than those in HMC.
444 Furthermore, the divergence between the THMC and the HMC simulation increases with time. In the
445 HMC simulation, after 50 years, Cd^{2+} concentration elevates to 50% of the source concentration level up
446 to 0.16 m depth of the liner, whereas in the THMC simulation the spread is up to 0.109 m, which shows
447 that the thermal mechanism has a great retardation effect on solute transport. That is an overprediction of
448 5.1 cm (31.9%) for a boundary temperature of 333 K (or $\Delta T = 40°C$). In HMC simulation, thermo-osmotic
449 consolidation and thermal diffusion are ignored, but the effects of mechanical loading, chemical-osmosis
450 and other processes remain unchanged.
451
452 **6. Conclusions**
453 In this paper, a fully coupled numerical model to study thermo-hydro-mechanical-chemical
454 behaviour of a saturated, semi-permeable clay soil, has been presented. The combined effect of thermo-
455 osmosis and chemical-osmosis on soil deformation and solute transport behaviour has been investigated.
456 Accuracy of the model in predicting the volume change behaviour and non-isothermal solute transport
457 has been demonstrated via partial validation exercises supported by laboratory data collected from the
458 literatures. In the application of the model, multiple loading events, e.g. mechanical loading, chemical
459 loading, and thermal loadings are simultaneously imposed on a natural clay liner with the intention to
460 identify the relative importance of thermo-osmotic consolidation on other loadings and to quantify its
461 impact on the overall deformation of the liner as well as on the spread of a representative solute such as
462 cadmium.
463 This study revealed that the effects of thermo-osmotic consolidation and the overall settlement of
464 the clay liner increases with temperature. A change in temperature from 40°C to 80°C resulted in an

increase of 11.3% of the peak settlement (from 24.71 mm to 27.55 mm), for the same simulation period. At the early stages, soil settlement is dominated by the mechanical loading and, in the long-term, both chemico-osmotic consolidation and thermo-osmotic consolidation are found regulating the deformation behaviours. Excess porewater pressure in semi-permeable clays increases with temperature. Ignoring the thermo-osmosis and/ thermo-osmotic consolidation processes in the simulations, the predicted transport significantly deviates from the realistic spread of the solute. Up to 80% overprediction of the spread of cadmium in the clay liner is observed when the thermo osmotic processes are neglected.

ACKNOWLEDGMENTS

Zhihong Zhang is supported by the Second Tibetan Plateau Scientific Expedition and Research (STEP) Program (No. 2019QZKK0905) and National Nature of Science Foundation of China (No. 51678012). Shakil A. Masum is supported by the Flexible Integrated System (FLEXIS) project funded by the Welsh European Funding Office (WEFO), Wales, UK. The financial supports are gratefully acknowledged.

References

Araujo ASD, Sonoda MT, Piro OE, et al. Development of new Cd^{2+} and Pb^{2+} lennard-jones parameters for liquid simulations. The Journal of Physical Chemistry (B), 2007, 111(9):2219-2224.

Barbour SL, Fredlund DG. Mechanisms of osmotic flow and volume change in clay soils. Canadian Geotechnical Journal, 1989, 26(4): 551-562.

Baldi G, Hueckel T and Pellegrini R. Thermal volume changes of the mineral-water in low-porosity clay soils. Canadian Geotechnical Journal, 1988, 25(4):807-825.

Carnahan C. Thermodynamic coupling of heat and matter flows in near-field regions of nuclear waste

repositories. MRS Online Proceedings Library Archive, 1983, 26:1983-1023.

Chen Y, Wang Y, Xie H. Breakthrough time-based design of landfill composite liners. Geotextiles and Geomembranes, 2015, 43(2): 196-206.

Chen Y, Xie H, Zhang C. Review on penetration of barriers by contaminants and technologies for groundwater and soil contamination control. Advances in Science and Technology of Water Resources, 2016,1(36):1-9.

Coo JL, So ZPS, Ng CWW. Effect of nanoparticles on the shrinkage properties of clay. Engineering Geology, 2016, 213:84-88.

Delage P, Sultan N, Cui YJ. On the thermal consolidation of Boom clay. Canadian Geotechnical Journal, 2000, 37(2):343-354.

Do N Y, Lee SR. Temperature effect on migration of Zn and Cd through natural clay. Environmental Monitoring and Assessment, 2006, 118(1-3): 267-291.

Donna AD, Laloui L. Response of soil subjected to thermal cyclic loading: Experimental and constitutive study. Engineering Geology, 2015, 190:65-76.

Ekbote, S and Abousleiman, Y. Porochemothermoelastic solution for an inclined borehole in a transversely isotropic formation, Journal of Engineering Mechanics, 2005, 131:522-533.

Francois B, Laloui L, Laurent C. Thermo-hydro-mechanical simulation of ATLAS in situ large scale test in Boom Clay. Computers and Geotechnics, 2009, 36(4):626-640.

Gao J, Deng J, Lan K, Song Z, Feng Y, Chang L. A porothermoelastic solution for the inclined borehole in a transversely isotropic medium subjected to thermal osmosis and thermal filtration effects. Geothermics, 2017, 67:114-34.

Gonçalvès J, Trémosa J. Estimating thermo-osmotic coefficient in clay rocks: I. Theoretical insights.

509 Journal of Colloid & Interface Science, 2010, 342:166-174.
510 Gonçalvès J, de Marsily G, Trémosa J. Importance of thermo-osmosis for fluid flow and transport in clay
511 formations hosting a nuclear waste repository. Earth & Planetary Science Letters. 2012, 339:1-10.
512 Habibagahi K. Temperature effect and the concept of effective void ratio. Indian Geotechnical Journal,
513 1977, 7(1): 14-34.
514 Hart RD, John CMS. Formulation of a fully-coupled thermal-mechanical-fluid flow model for non-linear
515 geologic systems. International Journal of Rock Mechanics and Mining Sciences & Geomechanics
516 Abstracts, 1986, 23(3): 213-224.
517 Huang L, Zhao CG, He J. Mixture theory based framework for transport of hydro-chemo-mechanical
518 solutes in landfills. Rock and Soil Mechanics, 2015, 36(1):47-55.
519 Hong PY, Pereira JM, Tang AM, et al. On some advanced thermo-mechanical models for saturated clays.
520 International Journal for Numerical and Analytical Methods in Geomechanics, 2013, 37(17):2952-
521 2971.
522 Kaczmarek M, Hueckel T, Chawla V, et al. Transport through a clay barrier with the contaminant concentration
523 dependent permeability. Transport in porous media, 1997, 29(2): 159-178.
524 Kaczmarek M, Hueckel T. Chemo-mechanical consolidation of clays: analytical solutions for a linearized
525 one-dimensional problem. Transport in Porous Media, 1998, 32(1):49-74.
526 Kaye G, Laby TH. Tables of physical and chemical constants. Harlow:Longman, 1986.
527 Keijzer TJS, Kleingeld PJ, Loch JPG. Chemical osmosis in compacted clayey material and the prediction
528 of water transport. Engineering Geology, 1997, 53(2):151-159.
529 Lewis T W, Pivonka P, Smith D W. Theoretical Investigation of the Effects of Consolidation on
530 Contaminant Transport through Clay Barriers. International Journal for Numerical & Analytical

Methods in Geomechanics, 2009, 33(1): 95-116.

Liu J, Wang H, Nie Y. Fractal model for predicting effective diffusion coefficient of solute in porous media. Advances in Water Science, 2004, 15(4): 458-462.

Lin Q. The adsorption and migration experimental research of heavy metals Cu, Cd, Pb, Zn in the soil. Qingdao University, 2008.

Lide, DR. CRC Handbook of Chemistry and Physics, CRC Press, Boca Raton, Florida, 1997.

Malusis MA, Shackelford CD. Theory for reactive solute transport through clay membrane barriers. Journal of Contaminant Hydrology, 2002, 59:291-316.

Malusis MA, Shackelford CD, Olsen HW. Flow and transport through clay membrane barriers. Engineering Geology, 2003, 70(3):235-248.

Malusis MA, Kang JB, Shackelford CD. Restricted salt diffusion in a geosynthetic clay line. Environmental Geotechnics, 2015, 2(2):68-77.

McVay GL, Scientific basis for nuclear waste management VII. Materials Research Society Symposium Proceedings, 1984, 26:513-520.

McTigue, D. Thermoelastic response of fluid-saturated porous rock, Journal of Geophysical Research, 1986, 91:9533-9542.

Mitchell JK, Witherspoon PA, Greenberg JA. Chemico-osmotic effects in fine-grained soils. Journal of the Soil Mechanics and Foundations Division, 1973, 99:307-322.

Mitchell, JK, Soga, K. Fundamentals of soil behaviour. 3rd Edition. Wiley, New York, 2005.

Monfared M, Sulem J, Delage P, Mohajerani M. On the THM behaviour of a sheared Boom clay sample: Application to the behaviour and sealing properties of the EDZ. Engineering Geology, 2012, 124:47-58.

553 Paaswell RE. Temperature effects on clay soil consolidation. Journal of the Soil Mechanics and
554 Foundations Division, 1967, 93(3): 9-22.
555 Peters GP, Smith DW. The influence of advective transport on coupled chemical and mechanical
556 consolidation of clays. Mechanics of Materials, 2004, 36(5):467-486.
557 Poulet T., Karrech A., Regenauer-Lieb K., Fisher L., and Schaubs P. Thermal-hydraulic-mechanical-
558 chemical coupling with damage mechanics using ESCRIPTRT and ABAQUS. Tetonophysics, 2012,
559 526-529:124-132.
560 Pu H, Fox P J, Shackelford C D. Assessment of consolidation-induced contaminant transport for
561 compacted clay liner systems. Journal of Geotechnical & Geoenvironmental Engineering, 2016,
562 142(3):113-124.
563 Robinet J-C, Rahbaoui A, Plas F, Lebon P. A constitutive thermomechanical model for saturated clays.
564 Engineering Geology, 1996, 41:145-169.
565 Roshan H, Andersen M, Acworth R. Effect of solid–fluid thermal expansion on thermo-osmotic tests: an
566 experimental and analytical study. Journal of Petroleum Science & Engineering, 2015, 126:222-230.
567 Sánchez M, Arson C, Gens A, Aponte F. Analysis of unsaturated materials hydration incorporating the
568 effect of thermo-osmotic flow. Geomechanics for Energy and the Environment, 2016, 6: 101-115.
569 Salomoni VA. A mathematical framework for modelling 3D coupled THM phenomena within saturated
570 porous media undergoing finite strains. Composites part B: Engineering, 2018, 146: 42-48.
571 Shackelford CD, Lu N, Malusis MA, Sample-Lord KM. Research challenges involving coupled flows in
572 geotechnical engineering. Geotechnical Fundamentals for Addressing New World Challenges,
573 Springer Series in Geomechanics and Geoengineering, Springer Nature, Switzerland AG, 2019, 237-
574 274.

575 Song Z, Liang F, Chen S. Thermo-osmosis and mechano-caloric couplings on THM responses of porous
576 medium under point heat source. Computers and Geotechnics. 2019, 112:93-103.
577 Soler JM. The effect of coupled transport phenomena in the Opalinus clay and implications for
578 radionuclide transport. Journal of Contaminant Hydrology, 2001, 53:63-84.
579 Smith DW, Booker JR. Green's functions for a fully coupled thermoporoelastic material. International
580 Journal for Numerical and Analytical Methods in Geomechanics, 1993, 17: 139-163.
581 Smith DW. One-dimensional contaminant transport through a deforming porous medium: theory and a
582 solution for a quasi-steady-state problem. International Journal for Numerical and Analytical Methods
583 in Geomechanics, 2000, 24(8): 693-722.
584 Sun HQ, Mašín D, Jan NJ, Najser J, Scaringi G. Water retention of a bentonite for deep geological
585 radioactive waste repositories: High-temperature experiments and thermodynamic modelling.
586 Engineering Geology, 2020, 269:105549.
587 Thomas HR, Cleall PJ Inclusion of expansive clay behaviour in coupled thermo hydraulic mechanical
588 models. Engineering Geology, 1997, 40(18): 3421-3441.
589 Trémosa J, Gonçalvès J, Matray JM, et al. Estimating thermo-osmotic coefficients in clay-rocks: II. In
590 situ experimental approach. Journal of Colloid & Interface Science, 2010, 342(1):175-184.
591 Tong F, Jing L, Zimmerman RW. A fully coupled thermo-hydro-mechanical model for simulating
592 multiphase flow, deformation and heat transfer in buffer material and rock masses. International Journal
593 of Rock Mechanics and Mining Sciences, 2010, 47(2): 205-217.
594 Villar MV, García-Siñeriz JL, Bárcena et al. State of the bentonite barrier after five years operation of an
595 in situ test simulating a high level radioactive waste repository. Engineering Geology, 2005, 80(3-
596 4):175-198.

597 Xie H, Zhang C, Sedighi M, et al. An analytical model for diffusion of chemicals under thermal effects
598 in semi-infinite porous media. Computers and Geotechnics, 2015, 69: 329-337.
599 Yang, Yang, Klaus Guerlebeck, and Tom Schanz. Thermo-Osmosis Effect in Saturated Porous Medium.
600 Transport in Porous Media, 2014, 104(2): 253-271.
601 Zhai X, Atefi-Monfared K. Explanation of early failure in porous media confined with flexible layers,
602 considering thermo-osmosis, thermal-filtration and heat sink from fluid dilation. Computer and
603 Geotechnics, 2020, 122, 103501.
604 Zhang Z, Masum SA, Thomas HR, et al. Modeling fully coupled hydraulic-mechanical-chemical
605 processes in a natural clay liner under mechanical and chemico-osmotic consolidation. Environmental
606 Science and Pollution Research, 2018, 25(36): 36173-36183.
607 Zheng L, Rutqvist J, Birkholzer JT, et al. On the impact of temperatures up to 200 °C in clay repositories
608 with bentonite engineer barrier systems: A study with coupled thermal, hydrological, chemical, and
609 mechanical modeling. Engineering Geology, 2015, 197:278-295.
610 Zheng L, Rutqvist J, Xu H, Birkholzer JT. Coupled THMC models for bentonite in an argillite repository
611 for nuclear waste: Illitization and its effect on swelling stress under high temperature. Engineering
612 Geology, 2017, 230:118-129.
613 Zhou Y, Rajapakse R, Graham J. A coupled thermoporoelastic model with thermo-osmosis and thermal-
614 filtration. International Journal of Solids and Structures, 1998, 35(34-35): 4659-4683.